

Effect of thermal treatment on the structural, morphological, and chemical properties of apatite bioceramics materials

N. E. Ghamri^a, O. K. Kribaa^{a,*}, L. Zenkhri^b, H. Djouama^a

^a*Applied chemistry laboratory, material sciences department, university Mohamed Khider Biskra, Algeria*

^b*Valorisation and Promotion of Saharan Resources laboratory (VPRS), Chemistry Department, Faculty of Mathematics and Material Sciences, Kasdi Merbah University, Ouargla, Algeria*

Monitoring the synthesis conditions of apatite phosphate by double decomposition seems very useful in view of the simplicity and rapidity of this method. This work is mainly based on production of apatite in the laboratory by the double decomposition method, HAP and TCP were synthesized and studied to demonstrate the influence of thermal treatment and synthesis temperature on the structure of apatite powders. The prepared samples were calcined at 900°C and sintered at 1050, 1100 and 1150°C. The effect of synthesis and sintering temperature on the structure of this material was investigated using XRD, FTIR, and SEM-EDX. This study confirmed that calcination has no effect on the HAP phase stability elaborated. Therefore, for TCP synthesized: β -TCP is the most phase that persists up to, 91% and a minimal partial transformation into Dicalcium Diphosphate is recorded. FTIR spectrum affirms the persistence of OH⁻ and PO₄³⁻ group bands suggesting the basic apatite structure for HAP and TCP of the sample, calcination, leads to the crystallization of TCP Ca₃(PO₄)₂. However, the calcined precipitate contains β calcium pyrophosphate Ca₂P₂O₇, and HA: Ca₁₀(PO₄)₆(OH)₂ constitutes secondary phase. While the calcination of HAP did not affect it. SEM micrograph of synthetic HAP powder treated at 1050°C revealed particle morphology with the dense and cloudy surface while TCP micrograph powder treated at the same temperature shows particle morphology of porous and smoother surfaces and irregular spherical shape. In conclusion thermal treatments improve the performance of the bioceramic residue and have the potential to create a new type of sustainable and bio-friendly material. Hydroxyapatite and tricalcium phosphate like other related calcium phosphate minerals, have been used extensively as orthopedic implant material due to their excellent biocompatibility and bone bonding to its structural and composition similarity to that of mineral phase of hard tissue in human bones.

(Received January 3, 2023; Accepted April 24, 2023)

Keywords: Apatite, Decomposition, Structure, HAP, TCP

1. Introduction

Like the most abundant mineral phosphate, apatite is a major component of industrial chemistry. In fact, the use of these compounds such as toothpaste pharmaceuticals, phosphors, anti-corrosion products, fuel additives, plasticizers, see pesticides, and other poisons and friction matches are essential to modern technological advances [1] Apatite is used as an additive in the treatment of contaminated soils and as back filling materials in the construction of radioactive waste containment barriers, these materials are also studied in archeology and paleontology [2]

Hydroxyapatite is extensively used in the medical and dental fields for bone redevelopment due to its bioactivity and biocompatibility properties. [3] Calcium phosphate cement (CPC) is a self-hardening synthetic cement and bone substitute material. CPCs are liquid and CaP-based powder phase systems that undergo a chemical reaction resulting in an arrangement of the material formed into a crystalline solid at body temperature. [4] CPCs can be

*Corresponding author: kribaokeltom@gmail.com
<https://doi.org/10.15251/DJNB.2023.182.531>

osteoconductive and their bioactive character allows integration into the tissue by the same processes involved in the remodeling of healthy bone. [5,6]

Among the varieties of these calcium phosphates, the two ceramics which retained the most attention are hydroxyapatite ($\text{Ca}_{10}(\text{PO}_4)_6(\text{OH})_2$) and phosphate tricalcium ($\text{Ca}_3(\text{PO}_4)_2$), known as TCP, as well as their mixtures [20, 21]. Phosphate tricalcium can be present in different forms, depending in particular on the temperature. Under the name generic TCP, we find the amorphous forms apatite (crystallography close to that of hydroxyapatite), β (rhombohedral), and α (monoclinic) [22,23]. The β -TCP phase is the most used and the most preferred given its good mechanical properties, its good fabric compatibility, and its ability to bond directly to the bone tissue without any middle connective tissue. [24, 25] Of more, rapid bone regeneration and appropriate speed of bioresorbability are other additional attributes of this phase [19, 23].

The sol-gel process is based on a controlled reaction mechanism in solution and generally at room temperature. These mechanisms rely on the conversion of liquid solutions (sols) into solid materials (dry gels called xerogels) through an inorganic polymerization process. [7] The precipitation method (wet chemical precipitation) [8, 9] is widely used in the wet method due to its simplicity.

In hydroxyapatite synthesized by chemical precipitation, many processes such as synthesis temperature, initial concentration of reactants involved in the reaction of a synthesis reaction, ambient temperature, etc., are required to obtain a product characterized by high purity and crystallinity. [10, 11]. The crystal structure of HAP belongs to the hexagonal system, with the space group $P6_3/m$, and the unit cell parameters of $a = b = 0.942 \text{ nm}$, $c = 0.688 \text{ nm}$, $\alpha = \beta = 90^\circ$, $\gamma = 120^\circ$ [12] Four calcium atoms are vertically distributed along c-axis are called Ca (I), and six calcium atoms arranged in a positive triangle around the c-axis are called Ca (II) [13]

During service as surgical implants, the mechanical resistance of β -TCP ceramics remains the most important parameter [14]. This depends on the density, grain size, morphology, grain boundary characteristics, etc. [15]. These structural and microstructural characteristics depend on the technique and conditions of synthesis and shaping technique. Usually, improving the mechanical resistance of ceramics is carried out by the densification-taking place during the sintering [14]. Sintering of β -TCP ceramics should be performed at a low temperature (below 1200°C) in order to avoid transformation into α -TCP [16, 17].

Obtaining pure TCP and HAP requires perfect control of the chemical composition during the preparation as well as the implementation of very precise characterization techniques. The major difficulty related to the synthesis of apatite TCP or HAP lies in the control of the rate of HPO_4^{2-} substitution in apatite depending on the synthesis parameters it seems necessary to specify the conditions allowing it to be obtained in such a way reproducible as possible.

The objective of this work is the synthesis of tricalcium phosphate and hydroxyapatite by the method of double decomposition, its ceramization, and the study of the effect of synthesis and sintering temperature of these bioceramics on the structural behavior.

2. Experimental

2.1. Synthesis of hydroxyapatite (HAP)

The preparation of hydroxyapatite ceramics requires the mixture of calcium hydroxide $\text{Ca}(\text{OH})_2$ and ammonium dihydrogen phosphate $(\text{NH}_4)_2\text{HPO}_4$, according to the Ca/P ratio of 1.67. The weighed powders were dissolved in a water-ethanol mixture with the ratio of 1:1 for calcium hydroxide and 1:2 for ammonium hydrogen phosphate in two separate bottles. Precipitation takes place by slow addition of PO_3^{4-} to the Ca^{2+} solution with continuous stirring for 1 h [18]. The HA suspension was left stirring for 24 h. A white solution was achieved. The $\text{pH} = 12$ during the process, the precipitate was separated from the suspension by vacuum filtration, washed with distilled water, ethanol, and then acetone. The precipitate was dried in an oven at 120°C for 24 hours and then ground. The next step is the calcination of powder obtained at 900°C for 2 h at a heating rate of $5^\circ\text{C}/\text{min}$ [18], sintered at a variety of temperatures: 1050, 1100, and 1150°C .

2.2. Synthesis tricalcium phosphate (TCP)

The synthesis of tricalcium phosphate powder was performed by the technique of double decomposition of two solutions: Solution A: $\text{Ca}(\text{NO}_3)_2 \cdot 4\text{H}_2\text{O}$ and Solution B: of $(\text{NH}_4)_2\text{HPO}_4$.

Solution B was added to solution A and the mixture is stirred for 30 min, under different temperatures (ambient, 70 and 90°C). The pH was adjusted to 7 by the gradual addition of an ammonia solution. The quantities of the reagents were taken in proportions stoichiometry (the Ca/P atomic ratio is equal to 1.5). The resulting precipitate was vacuum filtered and then rinsed abundantly with decarbonated water then dried in an oven at 80°C. Beta tricalcium phosphate (β -TCP) was prepared by calcination at 900°C for 2 h at a heating rate of 5°C/min. of the synthesized precipitate. Then it was crushed and homogenized in an agate mortar. The single-axial pressing (or compaction) formed the powder, and the samples were processed at 1050, 1100, and 1150°C for two hours.

2.3. Structural characterization

The physico-chemical characterization of the samples was carried out by Fourier transform infrared spectrometry (FTIR) and X-ray diffraction (XRD). The infrared spectrometric analysis of the samples was carried out using a SHIMADZU FTIR-8400S PC spectrometer with a wave number between 4000 and 600 cm^{-1} . The preparation of the pellets is carried out as 1mg of the powder to be analyzed is mixed with 0.2 g of dry KBr. X-ray diffraction spectra were obtained using a BRUKER D8 ADVANCE-XRD type counter diffractometer using radiation emitted by a copper anticathode ($\lambda = 1.54060 \text{ \AA}$), DRX diagrams are recorded in the 10°-70° interval (in 2 θ) with a step between 0.01 and 0.04°. The phases are identified by comparison with the references of the A.S.T.M.

2.4. Morphological characterization

This technique is based on the principle of electron-matter interactions; it is capable of producing high-resolution images of the surface of the sample. If a beam of primary electrons bombards a surface, several rays can be emitted For Scanning Electron Microscopy (SEM) analysis; the powder was in pellet form. A THERMO FISHER PRISMA E brand device is used for this study.

The EDX characterization of the layers was carried out within the University of Biskra Algeria. The EDX detector, associated with the SEM, makes it possible to perform quantitative surface chemical analyses. The detector is in the form of a silicon monocrystal partially compensated with lithium. Its adequate positioning (in our case, by crossing the surface of the sample at a distance of 10mm from the column outlet) makes it possible to collect a maximum of characteristic X photons, emitted during the change in the energy level of the electrons.

3. Results and discussions

We are interested in the Physico-chemical characterization of hydroxyapatite powders by different analysis techniques: X-ray diffraction (XRD), Fourier transforms infrared spectroscopy (FTIR), and morphological by scanning electron microscopy (SEM) coupled with energy-dispersive X-ray spectroscopy.

3.1. XRD characterization Of HAP and TCP

The X-ray diffraction patterns of the HAP powder synthesized and calcined at 900°C, sintered at 1050°C, 1100°C and 1150°C are shown in Figure 1 and The X-ray diffraction patterns of the TCP powder are shown in Figure 2.

The crystal lattice presents two types of tunnels noted "I" and "II", perpendicular to the plane (001). The type I tunnel is occupied by Me cations (Me I). In the case of HAP, it is Ca I. The sites of these cations are four in number per cell. They are placed on the ternary axes and are surrounded by nine oxygen atoms.

Type II tunnels contain the rest of the Me cations, six Me II cations per cell (Ca II in the case of HAP). These tunnels present a CS symmetry and the type II cations are localized in the periphery of this one. Grouped three by three at the levels $z = \frac{1}{4}$ and $z = \frac{3}{4}$ of the mesh, they form equilateral triangles shifted by 60° around the helical axis (axis c of the hexagonal mesh). With coordination equal to 7, six oxygen atoms of the tetrahedral groups XO₄ and the anionic group Y, surround them. [31, 32].

XRD results of TCP ceramics (Fig. 2) calcined at 900°C and sintered at different temperatures (1050, 1100 and 1150°C) show that: the Tricalcium Bis(orthophosphate) β -TCP phase is the phase that mostly persists up to 91% and a minimal partial transformation into Dicalcium Diphosphate(V) - Beta is recorded.

The patterns show that the powder of HAP is composed of phase "hydroxyapatite" of the chemical formula: $\text{Ca}_{10}(\text{PO}_4)_6\text{OH}_2$ which structure is Hexagonal (space group P6₃/m) with the following lattice parameters: $a=b=9,4260 \text{ \AA}$, $c = 6,8700 \text{ \AA}$. By comparing the three most intense hydroxyapatite spectrum lines obtained with that of the data from the A.S.T.M. files, we find that the most appropriate card for powder (see appendix) with the strongest lines.

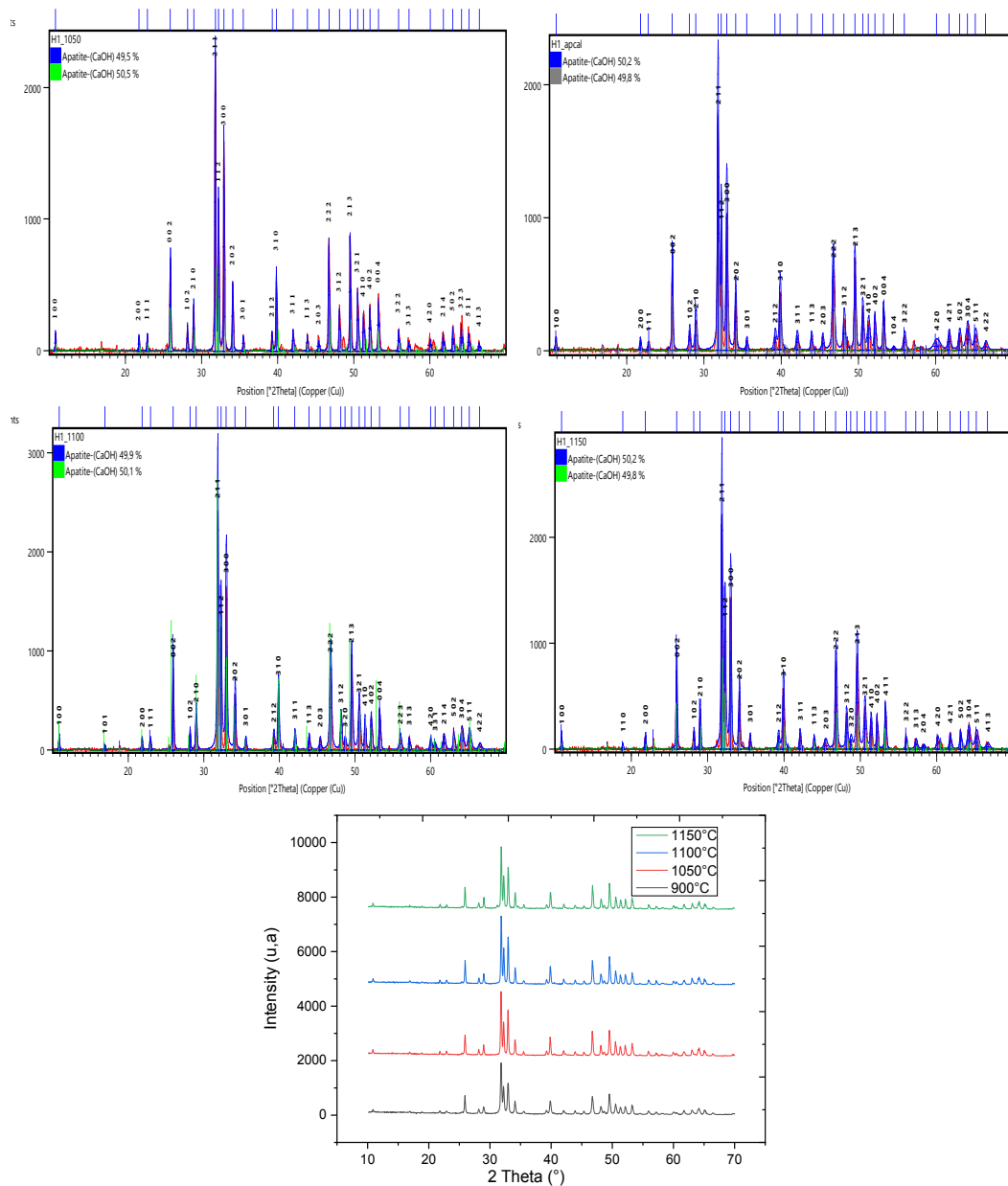


Fig. 1. X-ray diffraction patterns of the HAP.

For powder of TCP is composed of phases: Tricalcium Bis(orthophosphate) β -TCP (>91%) and Dicalcium Diphosphate (>8%). Tricalcium Bis(orthophosphate) β -TCP which structure is Hexagonal (space group R3c) with the following lattice parameters: $a = b = 10,4350 \text{ \AA}$. By comparing the three most intense hydroxyapatite spectrum lines obtained with that of the data from the A.S.T.M. files we find that the most appropriate card for our sample (see appendix).

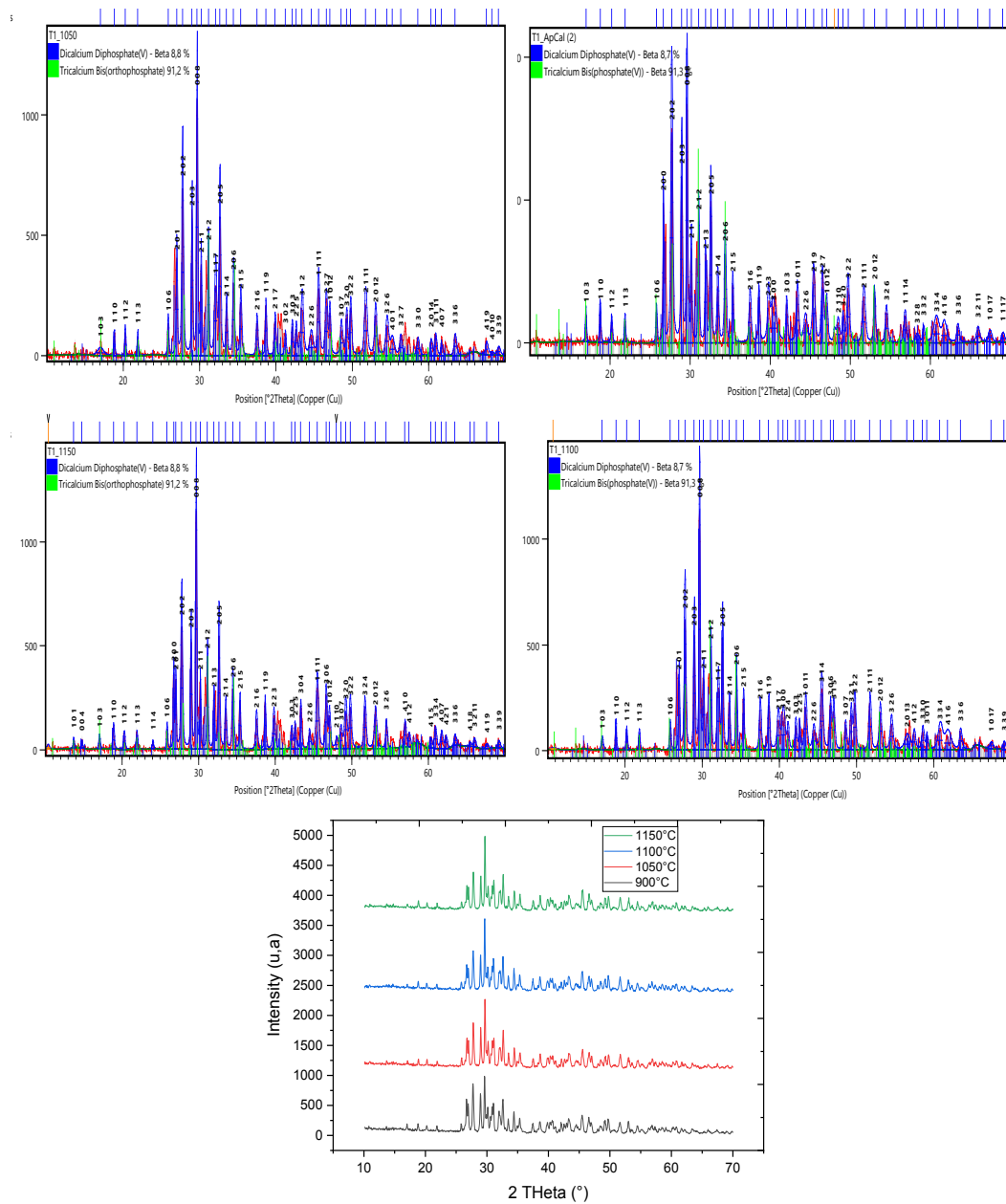


Fig. 2. X-ray diffraction patterns of the TCP.

From DRX diagrams, the crystallographic parameters are drawn for each composition, the information obtained grouped in the following table 1

Table 1. Crystallographic parameters for each composition.

HAP at 1150 °C	HAP at 1100 °C	HAP Calcined(at 900°C)
Crystal system: Hexagonal Space group: P 63/m a(Å): 9,4100 b(Å): 9,4100 c(Å):6,8790 Alpha(°):90,0000 Beta(°):90,0000 Gamma(°):120,0000 Calculated density(g/cm ³):3,16 Volume of cell (10 ⁶ pm ³):527,52	Crystal system:Hexagonal Spacegroup:P 63/m a (Å):9,4180 b (Å): 9,4180 c (Å):6,8840 Alpha (°): 90,0000 Beta (°): 90,0000 Gamma (°):120,0000 Calculated density (g/cm ³): 3,07 Volume of cell (10 ⁶ pm ³):528,80	Crystal system:Hexagonal Spacegroup:P 63/m a (Å):9,4260 b (Å):9,4260 c (Å):6,8650 Alpha (°):90,0000 Beta (°):90,0000 Gamma (°):120,0000 Calculated density (g/ cm ³):3,01 Volume of cell (10 ⁶ pm ³):528,23
HAP at1050 °C:	TCP Calcined at 900 °C	TCP at1100 °C
Crystal system:Hexagonal Spacegroup:P 63/m a (Å):9,4180 b (Å): 9,4180 c (Å):6,8840 Alpha (°): 90,0000 Beta (°): 90,0000 Gamma (°):120,0000 Calculated density (g/cm ³): 3,07 Volume of cell (10 ⁶ pm ³):528,80	Crystal system:Hexagonal Spacegroup:R 3 c a (Å):10,4350 b (Å):10,4350 c (Å):37,4030 Alpha (°):90,0000 Beta (°):90,0000 Gamma (°):120,0000 Calculated density (g/cm ³):3,07 Volume of cell (10 ⁶ pm ³):3527,13	Crystal system:Hexagonal Spacegroup:R 3 c a (Å): 10,4350 b (Å):10,4350 c (Å): 37,4030 Alpha (°): 90,0000 Beta (°): 90,0000 Gamma (°):120,0000 Calculated density (g/cm ³):3,07 Volume of cell (10 ⁶ pm ³):3527,13
TCP at1150°C	TCP at1050°C	
Crystal system:Hexagonal Spacegroup:R 3 c a (Å): 10,3630 b (Å): 10,3630 c (Å):37,2580 Alpha (°): 90,0000 Beta (°): 90,0000 Gamma (°):120,0000 Calculated density (g/cm ³): 3,12 Volume of cell (10 ⁶ pm ³):3465,14	Crystal system:Hexagonal Spacegroup:R 3 c a (Å): 10,3630 b (Å): 10,3630 c (Å): 37,2580 Alpha (°):90,0000 Beta (°): 90,0000 Gamma (°):120,0000 Calculated density (g/cm ³): 3,12 Volume of cell (10 ⁶ pm ³):3465,14	

3.2. IR spectra study Of HAP and TCP

The results of the analysis by absorption spectroscopy infrared (FTIR) of “TCP and HAP” synthesized before and after calcination at 900°C are shown in Figures 3 and 4.

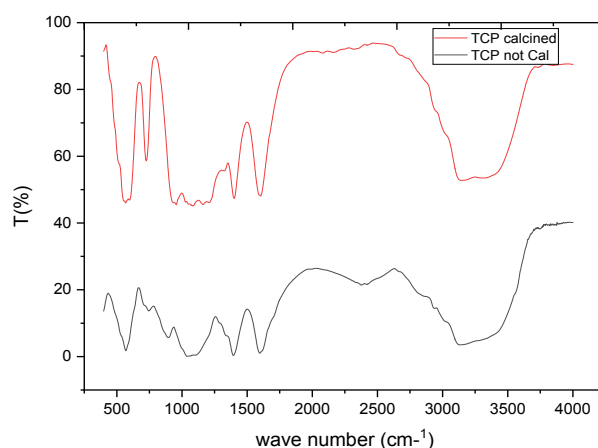


Fig. 3. FTIR spectrum of TCP.

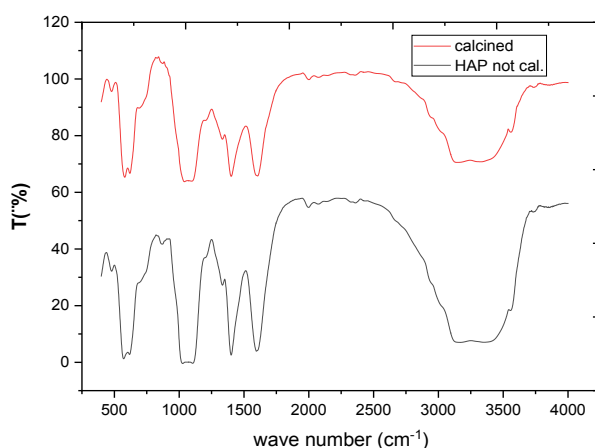


Fig. 4. FTIR spectrum of HAP.

According to the TF-IR spectra, we note the presence of the two intense bands the first is wide located between $3110 - 3449 \text{ cm}^{-1}$, and the other at 1613.34 cm^{-1} which are corresponding to the valence vibration of the O-H bond due to the presence of water in the solid network.

At 3542.02 cm^{-1} and at 695.29 cm^{-1} two fine and medium intensity bands corresponding to the stretching vibration of the O-H bond of the PAH. An intense fine band of the C-O bond of the CO_3^{2-} group is observed at 1411.79 cm^{-1} .

We also noticed the bands, which are attributed to the $(\text{PO}_4)^{3-}$ groupings of the following frequencies: $\nu_1 = 946.01 \text{ cm}^{-1}$, $\nu_2 = 473.49 \text{ cm}^{-1}$, $\nu_3 = 1015-1096 \text{ cm}^{-1}$ and $\nu_4 = 571, 85-613.32 \text{ cm}^{-1}$. We compared the results we obtained from TF-IR spectra of hydroxyapatite with other previous works (Table 2).

Table 2. Band indexing for 'HAP' IR spectra.

bands position in samples cm^{-1}	Band position Reference cm^{-1}	Intensity	Assignment	Ref
473.49	473	Strong	PO_4^{3-} symmetrical deformation: ν_2	[25]
571.85	565-600	Strong	PO_4^{3-} symmetrical deformation: ν_4	[26]
695.29	630	Mean	OH release band ν_1	[27]
/	873-885	Mean	CO_3^{2-} vibrational modes ν_2	[28]
946.01	962	Strong	PO_4^{3-} symmetric elongation ν_1	[29]
1015 – 1096	1043-1096	Strong	PO_4^{3-} antisymmetric elongation ν_3	[26]
1411.79	1415-1460	Mean	CO_3^{2-} vibrational modes ν_3	[28]
1613.34	1648	Strong	H_2O deformation of adsorbed water molecules	[26]
3110-3449	3456	Strong	OH H_2O elongation	[25, 26, 27]
3542.02	3573	Mean	OH symmetric elongation ν_s	[28][30]

By the comparison of the IR spectrum of the TCP powder before and after the calcinations at $T=900^\circ\text{C}$ presented on figure 3, we notice the appearance of the band located at 728 cm^{-1} , attributed to the grouping HPO_4^{2-} (P-OH elongation) and the disappearance of the band located at 2400 cm^{-1} , attributed to H_2O (symmetrical elongation of water molecules linked by bridges H). The calcination of apatitic TCP leads to the crystallization of TCP $\text{Ca}_3(\text{PO}_4)_2$. But the calcined precipitate contains β calcium pyrophosphate $\text{Ca}_2\text{P}_2\text{O}_7$ and, for a Ca/P molar ratio > 1.500 , the HA $\text{Ca}_{10}(\text{PO}_4)_6(\text{OH})_2$ constitutes the phase secondary. While the calcination of HAP has no effect, the pace of IR spectra is of the same pace.

All the results of the Fourier transform infrared spectrometry carried out on the precipitates obtained show that it is possible to obtain apatitic phosphate TCP and or HAP by the method of double decomposition in a water/ethanol medium, at $\text{pH}=7$ and at temperature $T=50^\circ\text{C}$. Phosphate apatitic tricalcium is identifiable by the characteristic bands of vibration of the PO_4^{3-} groups. During crystallization, the internal hydrolysis of a PO_4^{3-} group occurs simultaneously. Thus, a characteristic band HPO_4^{2-} groups is observed at 728 cm^{-1} .

3.3. Scanning electron microscopy (SEM)

The results of the scanning electron microscopy analysis of the materials are shown in the following figures, where : TCP synthesized at room temperature calcined and sintered at 1050°C on Figure 5. TCP synthesized at 70°C calcined and sintered at 1050°C on Figure 6. TCP synthesized at 90°C calcined and sintered at 1050°C on Figure 7. HAP synthesized at room temperature calcined and sintered at 1050°C on Figure 8, HAP synthesized at room temperature calcined and sintered at 1100°C on Figure 9 and HAP synthesized at room temperature calcined and sintered at 1150°C on Figure 10

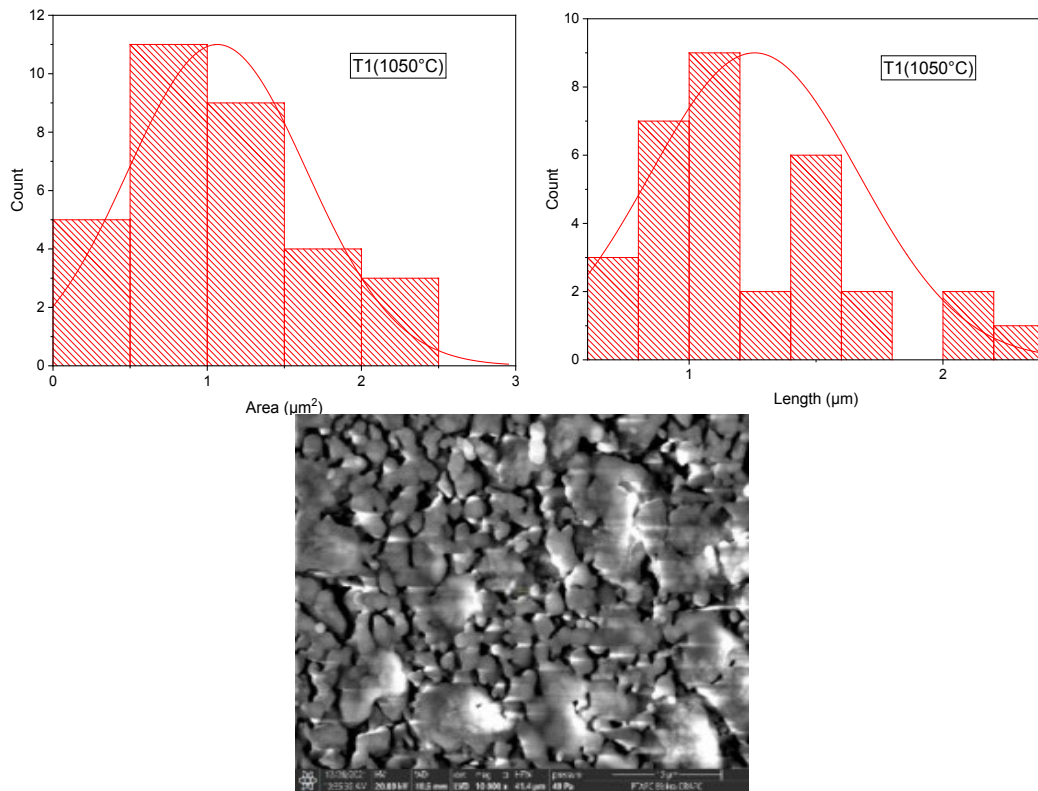


Fig. 5. Length and area histogram, microscopic photo of TCP synthesized at room temperature sintered at 1050°C.

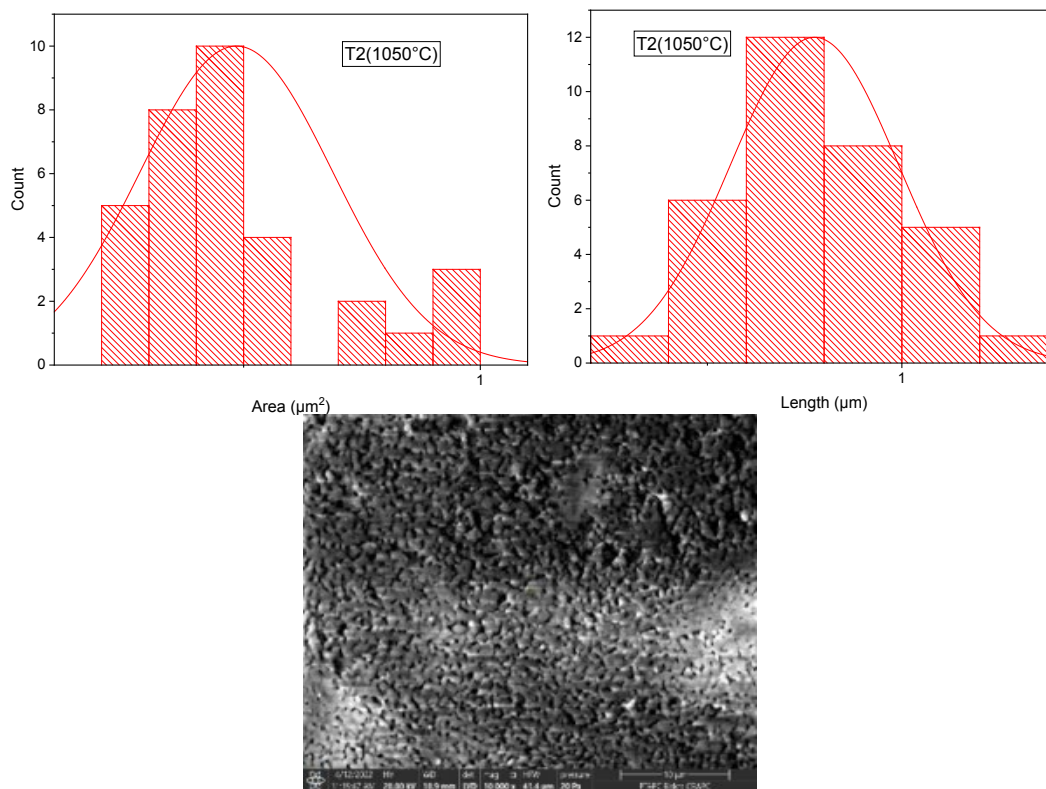


Fig. 6. Length and area histogram, microscopic photo of TCP synthesized at 70°C sintered at 1050°C.

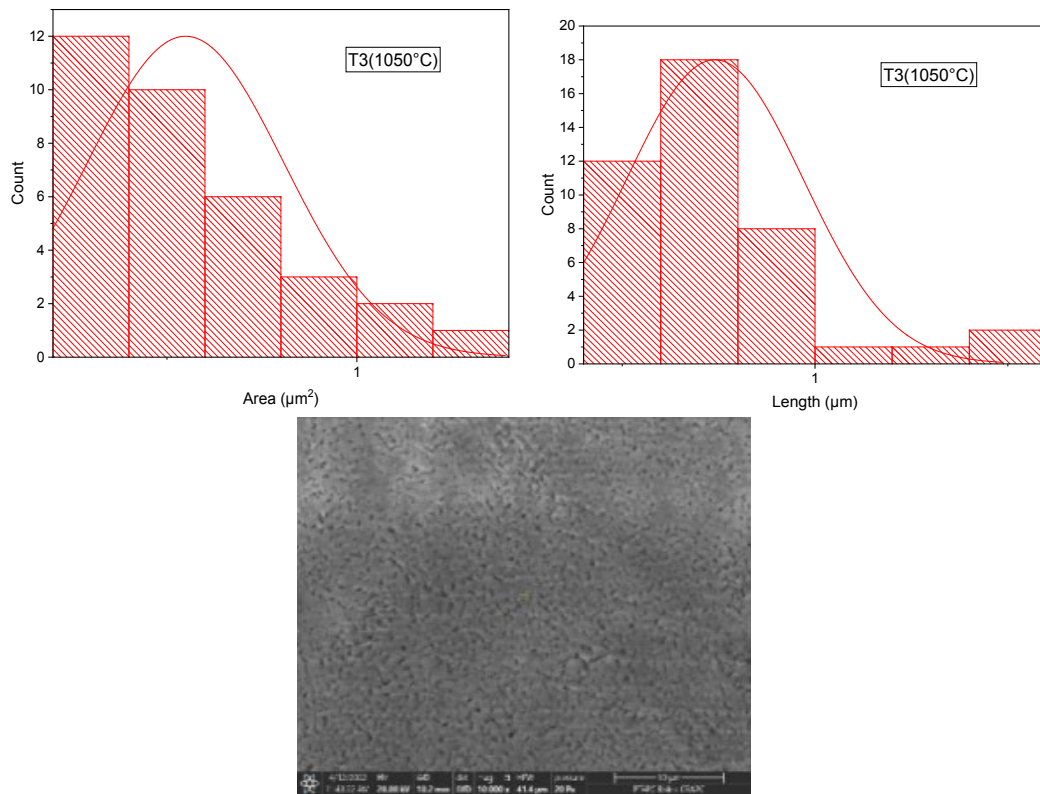


Fig. 7.Length and air histogram, microscopic photo of TCP synthesized at 90°C sintered at 1050°C.

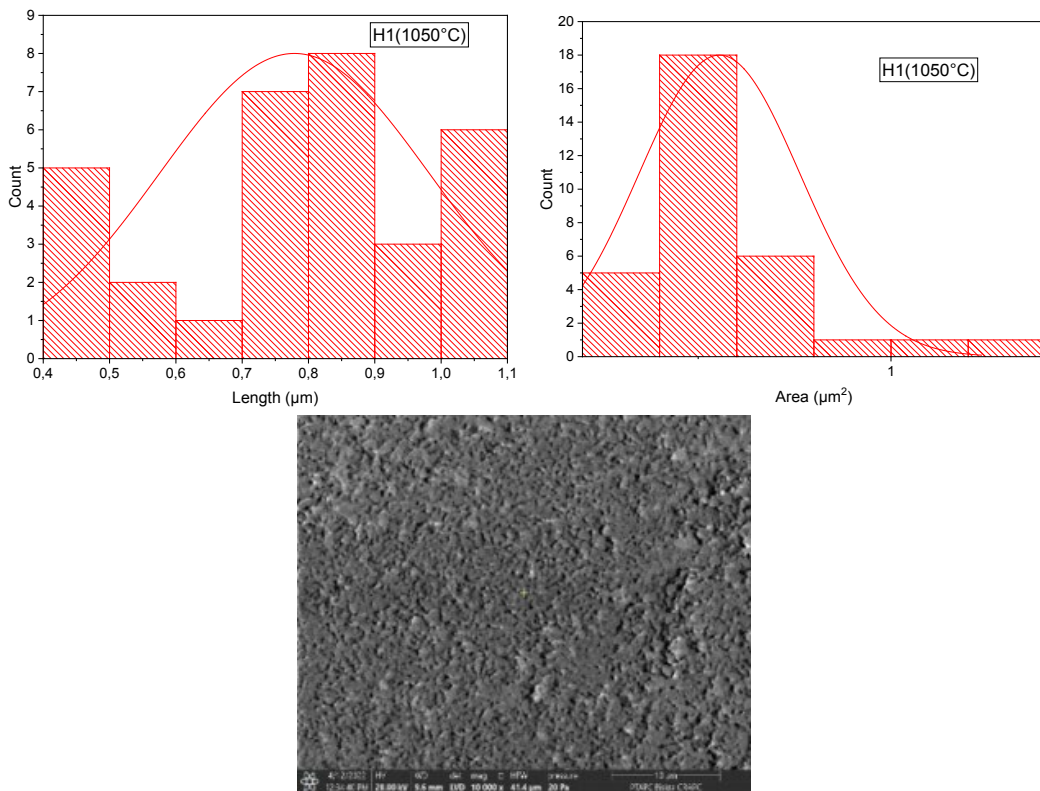


Fig.8.Length and air histogram, microscopic photo of HAP synthesized at room temperature sintered at 1050°C.

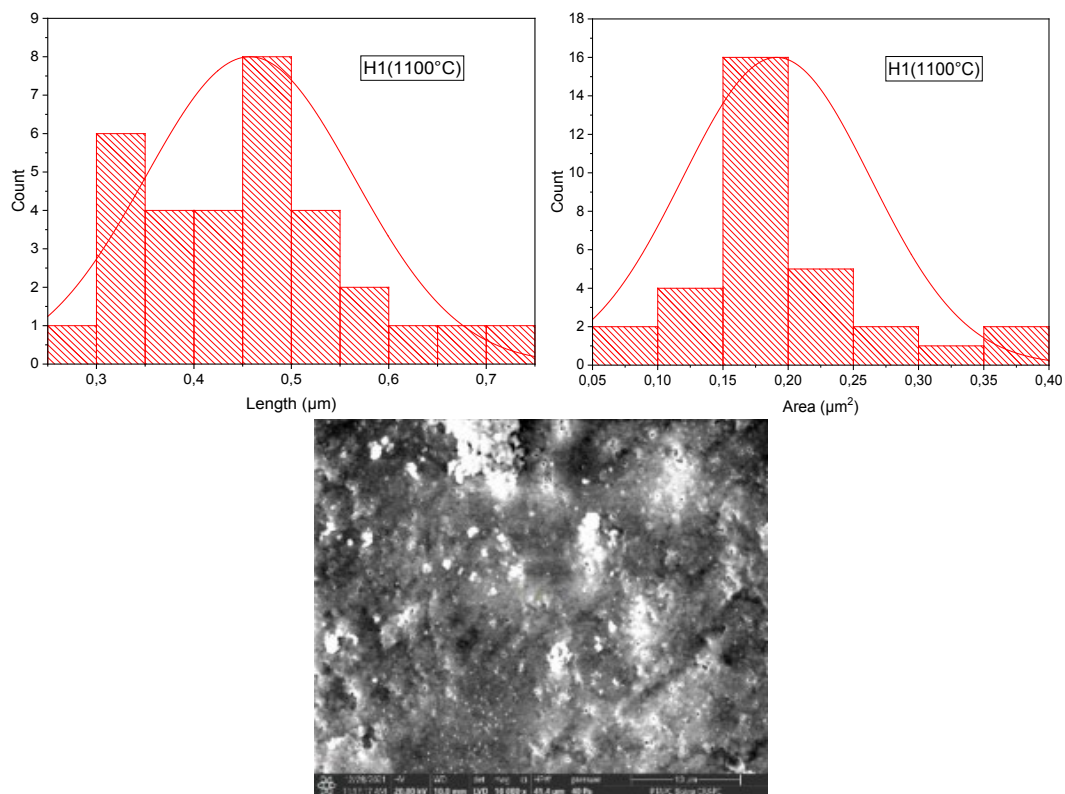


Fig.9.Length and air histogram, microscopic photo of HAP synthesized room temperature sintered at 1100°C.

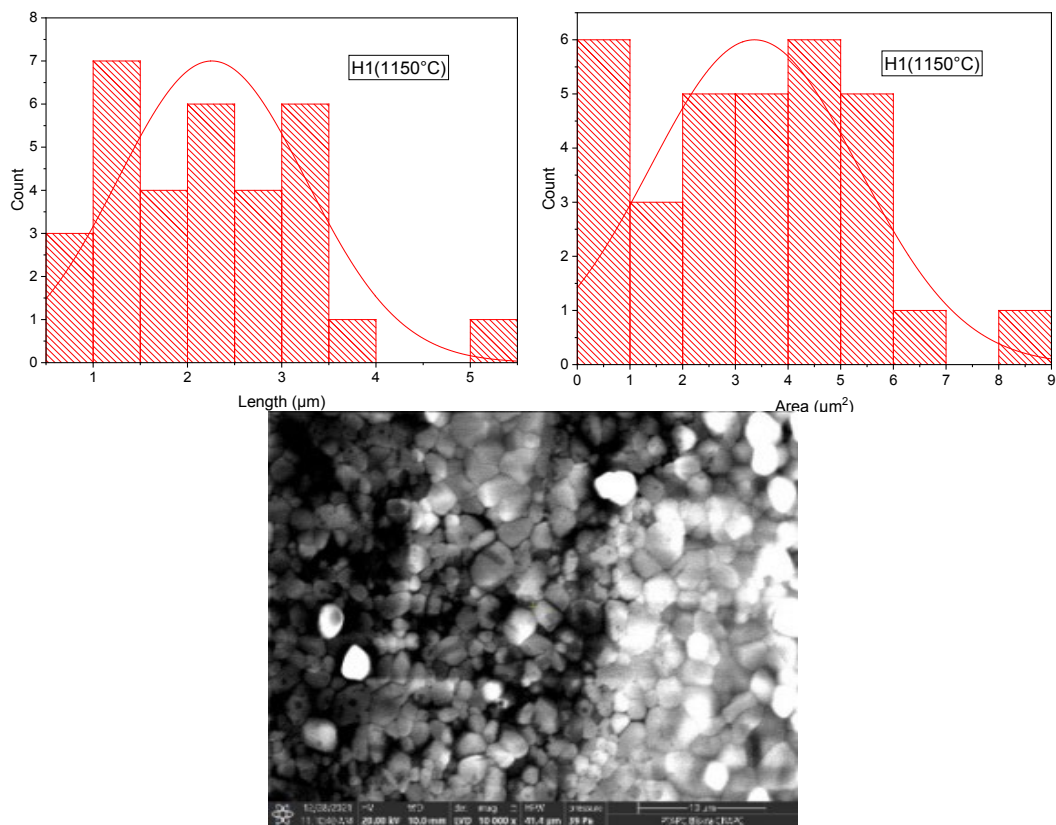


Fig.10. Length and air histogram, microscopic photo of HAP synthesized at room temperature sintered at 1150°C.

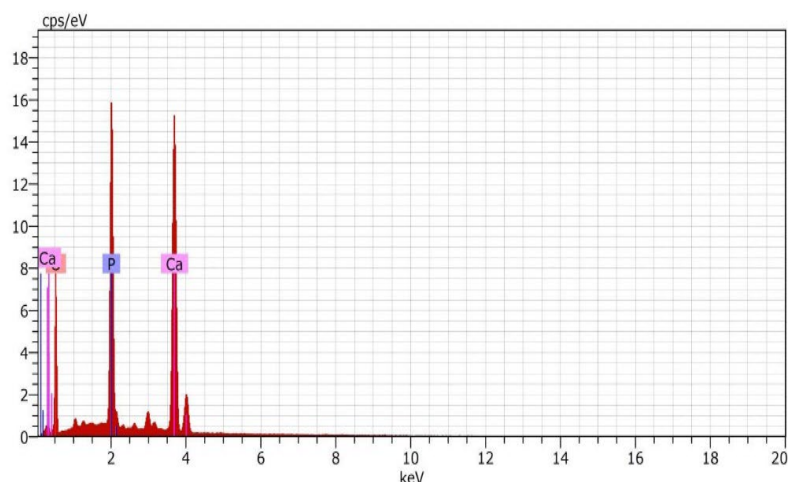


Fig.11. Pattern of synthetic HA calcined at 900°C.

From the SEM micrograph of the synthesized hydroxyapatite powder heat-treated at 1050 °C (Fig.8), we can see the appearance of regular dense powder particles with no vacancies between them. The SEM of synthetic HA heat-treated at 1100 °C and 1150 °C (Figure 9, 10) revealed a crystallized and porous model, with an irregular, oval and spherical shape resembling lozenges. We also note the increase in the length and the area of the grains with an increase in the sintering temperature. Whereas for TCP presented in figures 5,6 and 7 calcined at the same temperature 1050 °C, synthesized at different temperatures (ambient, 70, and 90 °C), we note the reduction in size and the air of the grains with synthesis temperature, the structure revealed a poorly crystallized, dense model and a regular spherical shape.

The architecture of the material must be adapted as needed. The presence of pores interconnected allows the development of vascularization and facilitates colonization of cells in the material. Bone growth is then favored, which generates better biological fixation of the implant [31].

According to the energy-dispersive X-ray spectroscopy spectra (Fig.11), the predominant elements in both samples are P and Ca without any sign of impurities. Note the existence of two types of calcium, which confirms the results obtained by DRX (two types of Apatite-CaOH)

4. Conclusion

In this work, HAP and TCP were synthesized using the method of double decomposition, to demonstrate the influence of thermal treatment and synthesis temperature on the structure of apatite powders. The prepared samples were calcined at 900 °C, and the effect of synthesis and sintering temperature on the structure of this material was investigated using XRD, FTIR, and SEM-EDX.

The XRD diagrams of the hydroxyapatite HAP powder synthesized calcined at 900 °C and sintered at 1050 °C, 1100 °C, and 1150 °C clearly represent the hydroxyapatite phase. This study confirmed that calcination has no effect on the phase stability of HAP (absence of secondary phases).

XRD diagrams of TCP powder calcined at 900 °C and sintered at different temperatures (1050, 1100, and 1150 °C) show that: β TCP is the phase that mostly persists up to 91%, and a minimal partial transformation into Dicalcium Diphosphate is recorded.

From the FTIR spectrum, it was observed that the persistence of the OH^- and PO_4^{3-} group bands suggests the basic apatite structure for HAP and TCP of the sample, by the calcination.

SEM micrograph of synthetic HAP powder treated at 1050 °C revealed particle morphology with the dense and cloudy surface while the micrograph of TCP powder treated at the same temperature 1050 °C shows particle morphology of porous (voids found between particles)

and smooth surfaces and an irregular spherical shape. We note the increase in the length and the area of the grains with an increase in the sintering temperature and decrease with an increase in the synthesis temperature

Abbreviations

HAP: Hydroxyapatite.

TCP: Tricalcium phosphate

CaP: Calcium Phosphate.

ASTM: American Society for Testing Materials.

JCPDS: Journal of compound Powder diffraction society.

Appendix A. HAP calcined

Visible	Ref. Code	Score	Compound Name	Displacement [°2Th.]	Scale Factor	Chemical Formula
*	98-015-2194	85	Apatite-(CaOH)	0,000	0,766	H5.88 Ca9.77 O27.3 P3
*	98-008-1442	39	Apatite-(CaOH)	0,000	0,346	H1 Ca5 O13 P3

Appendix B. HAP 1050

Visible	Ref. Code	Score	Compound Name	Displacement [°2Th.]	Scale Factor	Chemical Formula
*	98-015-4493	91	Apatite-(CaOH)	0,000	0,716	H0.876 Ca5.082 O12.282 P2.817
*	98-008-1442	50	Apatite-(CaOH)	0,000	0,264	H1 Ca5 O13 P3

Appendix C. HAP1100

Visible	Ref. Code	Score	Compound Name	Displacement[°2Th.]	Scale Factor	Chemical Formula
*	98-005-6306	81	Apatite-(CaOH)	0,000	0,717	H1 Ca5 O13 P3
*	98-002-4240	46	Apatite-(CaOH)	0,000	0,936	H1 Ca5 O13 P3

Appendix D. HAP1150

Visible	Ref. Code	Score	Compound Name	Displacement [°2Th.]	Scale Factor	Chemical Formula
*	98-005-6306	83	Apatite-(CaOH)	0,000	0,722	H1 Ca5 O13 P3
*	98-008-1442	35	Apatite-(CaOH)	0,000	0,291	H1 Ca5 O13 P3

Appendix E. TCP calcined

Visible	Ref. Code	Score	Compound Name	Displacement [°2Th.]	Scale Factor	Chemical Formula
*	98-001-4313	65	DicalciumDiphosphate(V) - Beta	0,000	0,950	Ca2 O7 P2
*	98-041-7500	47	TricalciumBis(orthophosphate)	0,000	0,625	Ca3 O8 P2

Appendix F. TCP1050

Visible	Ref. Code	Score	Compound Name	Displacement [°2Th.]	Scale Factor	Chemical Formula
*	98-001-4313	52	DicalciumDiphosphate(V) - Beta	0,000	0,524	Ca2 O7 P2
*	98-041-0782	31	TricalciumBis(orthophosphate)	0,000	0,376	Ca3 O8 P2

Appendix G. TCP1100

Visible	Ref. Code	Score	Compound Name	Displacement [°2Th.]	Scale Factor	Chemical Formula
*	98-001-4313	64	DicalciumDiphosphate(V) - Beta	0,000	0,729	Ca2 O7 P2
*	98-041-0782	44	TricalciumBis(orthophosphate)	0,000	0,428	Ca3 O8 P2

Appendix H. TCP1150

Visible	Ref. Code	Score	Compound Name	Displacement [°2Th.]	Scale Factor	Chemical Formula
*	98-001-4313	55	DicalciumDiphosphate(V) - Beta	0,000	0,498	Ca ₂ O ₇ P ₂
*	98-041-0782	26	TricalciumBis(orthophosphate)	0,000	0,310	Ca ₃ O ₈ P ₂

References

- [1] D. B. S. McConnel, M. S, Technische Mineralogie Springer-Verlag Wien, 5, (1973).
- [2] A-M. Pollard, C. Heron, Second Edition 2008, The Royal Society of Chemistry ; <https://doi.org/10.1039/9781847558299-FP009>
- [3] M. Raghavendra, K. Varaprasad T. Jayaramudu, 21-44, (2015) ; <https://doi.org/10.1016/B978-0-323-32889-0.00002-9>
- [4] I. L. Torrecilla, J.J.J.P. V. D. Beuckena, J. A. Jansena, Acta Biomaterialia, 119, 1(2021)
- [5] H. Yuan, Y. Li, J. De Bruijn, K. De Groot, X. Zhang, Biomaterials, 21(12), 1283(2000). [https://doi.org/10.1016/S0142-9612\(00\)00016-8](https://doi.org/10.1016/S0142-9612(00)00016-8)
- [6] F. Pupilli, A. Ruffini, M. Dapporto, M. Tavoni, A. Tampieri, S. Sprio, Design Strategies and Biomimetic Approaches for Calcium Phosphate Scaffolds in Bone Tissue Regeneration, 7(3), 112(2022) ; <https://doi.org/10.3390/biomimetics7030112>
- [7] M. S. Shojai, S. S. Khorasani, M. Khoshdargi, D. Jamshidi, Acta biomaterialia 9(8), 759 (2013).
- [8] S.V. Dorozhkin, Acta Biomater 6(3), 715(2010) ; <https://doi.org/10.1016/j.actbio.2009.10.031>
- [9] M. P. Ferraz, F. J. Monteiro, C. M. Manuel, Appl Biomater Biomech 2(2).74(2004).
- [10] N. Angelescu, D. Ungureanu, F. Anghelina, Sci Bull Valahia Univ Mater Mech 6, 15 (2011).
- [11] S. Pramanik, A. K. Agarwal, K. N. Rai. A. Garg, Ceramics International 33(3), 419(2007) ; <https://doi.org/10.1016/j.ceramint.2005.10.025>
- [12] M. Qi, K. He, Z. Huang, et al., a Review of synthesis methods 69 (8) 1354 (2017) ; <https://doi.org/10.1007/s11837-017-2427-2>
- [13] J.D. Pasteris, B. Wopenka, E. Valsami-Jones 4(2), 97(2008) ; <https://doi.org/10.2113/GSELEMENTS.4.2.97>
- [14] B. Chen, Z. Zhang, J. Zhang, Q. Lin, D. Jiang, Mat. Sci. Eng C. 28 1052(2008) ; <https://doi.org/10.1016/j.msec.2007.04.034>
- [15] K. Lin, J. Chang, J. Lu, W. Wu, Y. Zeng, Int 33, 979(2007) ; <https://doi.org/10.1016/j.ceramint.2006.02.011>
- [16] D. Choi , P. N. Kumta, Mat. Sci. Eng. C 27, 377(2007) ; <https://doi.org/10.1016/j.msec.2006.05.035>
- [17] M. Descamps, J.C. Hornez, A. Leriche, J. Eur. Ceram. Soc. 27(6), 2401(2007) ; <https://doi.org/10.1016/j.jeurceramsoc.2006.09.005>
- [18] O. K. Kribaa, S. Latif, F. Saifi, N. Chahbaoui, polyethylene 49, 1017(2022) ; <https://doi.org/10.1016/j.matpr.2021.08.120>
- [19] G. B. M. Ribeiro, R. M. Trommer, L. A. dos Santos, C. P. Bergmann, Mater. Lett 65, 275(2011) ; <https://doi.org/10.1016/j.matlet.2010.09.066>
- [20] S-H. Kwon, Y-K. Jun, S-H. Hong, H-E. Kim, Eur. Ceram. Soc 23, 1039(2003) ; [https://doi.org/10.1016/S0955-2219\(02\)00263-7](https://doi.org/10.1016/S0955-2219(02)00263-7)
- [21] M. Jarcho, Clin. Orthop 157, 259(1981) ; <https://doi.org/10.1097/00003086-198106000-00037>
- [22] J. Chevalier, Sciences et technologies céramiques, Publication du Groupe français de la céramique, Edition EDP science 639 (2009).
- [23] D. Choi, P. N. Kumta, Mat. Sci. Eng C 27, 377(2007) ;

<https://doi.org/10.1016/j.msec.2006.05.035>

[24] B. Chen, Z. Zhang, J. Zhang, Q. Lin, D. Jiang, *Mat. Sci. Eng C* 28, 1052(2008) ;

<https://doi.org/10.1016/j.msec.2007.04.034>

[25] A. Costescu, I. Pasuk, F. Ungureanu, A. Dinischiotu , M. Costache , F. Huneau , S. Galaup, P. LE coustumer, D. Predoi, *Digest Journal of Nanomaterials and Biostructures* 5 (4), 989(2010).

[26] S. Markovic, L. Veselinović, M J. Lukić, L. Karanović, I. Bracko, N. Ignjatovic, D. Uskokovic, *Biomed. Mater*, 6, No. 045005(2011)

[27] B.O. Fowler, Reaction of methylchlorophosphine with some simple boron compounds, *journal Inorg. Chem* 13, 194(1974) ; <https://doi.org/10.1021/ic50131a033>

[28] J. S. Silva, T. R. Machado, T. A. Martins, M. Assis, C. C. Foggi, N. G. Macedo, H. B. Mir E. Cordoncillo, J. A. E. Longo, *Société américaine de Chimie inorganique*. 58, 5900(2019) ;

<https://doi.org/10.1021/acs.inorgchem.9b00249>

[29] K. Himanshu, P. Satya, *Journal of Minerals and Materials Characterization and Engineering* 4, 119(2016).

[30] C.V. Blitterswijk, P. Thomsen, « Tissue engineering ». Elsevier, Acad. Press. United States of America (2008).

[31] G. Montel, G.B. J.-C. Trombe, J-Claude Heughebaert, C. Rey, *Pure & Appl. Chem.*, 52, pp. 973-987(1980) ; <https://doi.org/10.1351/pac198052040973>

[32] M. I. Kay, R.A.Y, and A. S. Posner, *Nature*,(1964), Crystal structure of hydroxyapatite,204, pp. 1050- 1052 ; <https://doi.org/10.1038/2041050a0>